Hindawi
Mathematical Problems in Engineering
Volume 2019, Article ID 1013025, 14 pages
https://doi.org/10.1155/2019/1013025

Research Article

Flutter Performance of the Emergency Bridge with New-Type Cable-Girder

Lei Yang, Fei Shao, Qian Xu, and Ke-bin Jiang

College of Field Engineering, Army Engineering University of PLA, Nanjing 210007, China

Correspondence should be addressed to Fei Shao; shaofei@seu.edu.cn and Qian Xu; 1058427910@qq.com

Received 21 January 2019; Revised 21 February 2019; Accepted 27 February 2019; Published 17 March 2019

Academic Editor: Giuseppe Vairo

Based on the proposed emergency bridge scheme, the flutter performance of the emergency bridge with the new-type cable-girder has been investigated through wind tunnel tests and numerical simulation analyses. Four aerodynamic optimization schemes have been developed in consideration of structure characteristics of the emergency bridge. The flutter performances of the aerodynamic optimization schemes have been investigated. The flutter derivatives of four aerodynamic optimization schemes have been analyzed. According to the results, the optimal scheme has been determined. Based on flutter theory of bridge, the differential equations of flutter of the emergency bridge with new-type cable-girder have been established. Iterative method has been used for solving the differential equations. The flutter analysis program has been compiled using the APDL language in ANSYS, and the bridge flutter critical wind speed of the optimal scheme has been determined by the program. The flutter analysis program has also been used to determine the bridge flutter critical wind speed of different wind-resistance cable schemes. The results indicate that the bridge flutter critical wind speed of the original emergency bridge scheme is lower than the flutter checking wind speed. The aerodynamic combined measurements of central-slotted and wind fairing are the optimal scheme, with the safety coefficients larger than 1.2 at the wind attack angles of -3°, 0°, and $+3^\circ$. The bridge flutter critical wind speed of the optimal scheme has been determined using the flutter analysis program, and the numerical results agree well with the wind tunnel test results. The wind-resistance cable scheme of 90° is the optimal wind cable scheme, and the bridge flutter critical wind speed increased 31.4%. However, in consideration of the convenience in construction and the effectiveness in erection, the scheme of wind-resistance cable in the horizontal direction has been selected to be used in the emergency bridge with new-type cable-girder.

1. Introduction

As compared to normal bridges, the emergency bridge has the characteristics of small stiffness and damping. It is a wind-sensitive structure, which is prone to a variety of wind-induced vibrations. Generally, the torsional stiffness of the combined plate beam in a suspension bridge is smaller than that of a box girder or a truss girder. For the Tacoma Narrows Bridge, the combined plate beam was used, and the collapse of the bridge was the result of not considering the flutter stability in the design [1]. In consideration of the demand in transportation and erection, the combined plate beam type is still used widely in emergency bridge structure. In China, the maximum single span of an emergency bridge is 51 m, which cannot satisfy the demand of rescue and relief works in mountainous areas. In order to satisfy the demand, in this study, using a new-type cable-girder, an emergency bridge which can span 150 m has been developed. The light weight, high strength fiber cable has been used as the main cable. The combined plate beam has been used as the main girder, and the splicing structure has been used as the pylon. Therefore, the stiffness of the emergency bridge with new-type cable-girder is relatively low. Further, as the wind resistibility of the combined plate beam is not strong, therefore the flutter of the emergency bridge is worth studying.

Dung [2] and Ge [3] developed the mode superposition method for flutter analysis of a suspension bridge. The advantage of this method is that the full participating natural modes of vibration can be considered, but the calculation is time-consuming. However, the mode superposition method is commonly used due to its accuracy and efficiency. Jones and Scanlan [4], Jain [5], and Tanaka [6] utilized the determinant search method directly to predict the bridge flutter critical condition. In recent years, with the development of

computers, numerical simulation studies are widely used in flutter analysis. Flutter derivatives are the key parameter for numerical analysis of flutter, and different turbulence models had been used for obtaining the flutter derivatives of bridge cross-section. Vairo [7, 8] proposed a numerical model based on a finite volume ALE formulation and employs a k-ε turbulence model; the accuracy and applicability of the model to wind engineering problems were successfully assessed by computing the aerodynamic behaviour of simple cross-section shapes and typical cross-sections. The effectiveness of the sst (shear-stress-transport) and the standard (std) RANS-based turbulence models in predicting flutter derivatives had been compared, and the k-ε sst formulation proved to be more accurate than the k-ε std [9]. A 2D unsteady Reynolds-averaged Navier-Stokes (URANS) approach adopting Menter's SST k-ε turbulence model was employed for computing the flutter and the static aerodynamic characteristics, and the conclusions indicated that the results provided by the proposed methodology agree well with the experimental data [10]. The performances of standard Smagorinsky-Lilly and Kinetic Energy Transport turbulence models were applied to study the unsteady flow field around a rectangular cylinder [11]. The accuracy of standard computational fluid dynamics techniques and turbulence models in predicting the critical flutter speed of streamlined and bluff deck sections was investigated, and the results showed that the flutter onset velocity had mainly been underestimated but cases showing opposite behavior [12]. By considering the nonlinear wind-structure interactions based on the linear theory, Zhang [13] developed an approach for the aerostatic and aerodynamic analysis. Based on ANSYS, Hua [14] developed an approach for the full-mode aerodynamic flutter analysis. The method of full-mode aerodynamic flutter analysis was used to analyze the aerodynamic flutter analysis of a suspension with double main spans [15]. A simple analytical approach to aeroelastic stability problem was proposed and had been proved to be consistent and effective for successfully capturing the main wind-bridge interaction mechanisms [16]. Bai [17] carried out a study on the flutter stability of a steel truss girder suspension bridge. Wind tunnel tests were performed to investigate the effects of different aerodynamic measures on the flutter stability of a steel truss girder suspension bridge. PC slab stiffening girder section is similar to the combined plate beam. These section types are not strong in wind resistibility of structure. Zhu [18] analyzed the flutter stability of a suspension bridge with PC slab stiffening girder. The results showed that the suspension bridge with PC slab stiffening girder was sensitive to the wind attack angles. Based on a series of wind tunnel tests, Yang [19] investigated the influence of vertical central stabilizers on the flutter performance of twin-box girders. Based on wind tunnel tests and computational fluid dynamics (CFD) simulations, a study on the flutter performance of twin-box bridge girders at large angles of attack was presented [20].

On the energy viewpoint of flutter, bridge structure can absorb energy from the wind-induced vibration. Energy harvesting from wind-induced vibrations of long-span bridges through electromagnetic devices was studied [21]. The coupling vibrations have attracted the researchers' attention. The phenomena of RIWVs were reproduced using a high-precision simulator, and the effects of wind speed and rain were considered by wind tunnel tests [22]. The accuracy of wind tunnel test is a key question for wind-induced vibration of bridge. Fabio [23] investigated experimental error propagation, and three different experimental data sets had been used in studying the effects on critical flutter speeds of pedestrian suspension bridge.

There are only a few studies on the wind-resistance of emergency bridges [24]. In this study, using wind tunnel tests and numerical simulation analyses, the wind-resistance performance of the emergency bridge has been investigated. The results can be used as a reference for other similar studies.

2. Emergency Bridge with New-Type Cable-Girder

2.1. Description of the Emergency Bridge with New-Type Cable-Girder. The emergency bridge with the new-type cable-girder comprises of the cable system, the girder, the pylon, and the anchorage system. The emergency bridge is allowed to carry 35 tons of pedrail deck load and 13 tons of wheel load. The emergency bridge has a span of 150 m. The height of the pylon is 15 m. The sag-span ratio is 1/12, and the height of the girder is 0.75 m. The cable system comprises of cable and suspender. The entire bridge has two cables which are in the straddle form. The material of the suspender is round steel. The lateral distance between suspenders is 6 m, and the suspender is anchored to the main beam. The longitudinal distance between suspenders is 10 m. The pylon is assembled by the aluminum alloy profile of H-type, and the type of aluminum alloy is 7005. The main girder mainly consists of three parts: main girder, cross beam, and spandrel beam. Curbs are installed outside of the main girder. A sketch of the bridge is shown in Figures 1 and 2. The section of main girder is shown in Figures 3 and 4.

2.2. Dynamic Characteristic of the Emergency Bridge. Based on a quasi-secant large-displacement formulation, a nonlinear continuous model for the analysis of long-span cable-stayed bridges was proposed; the model opens the possibility to develop more refined closed-form solutions for the analysis of cable-stayed structures [25]. In order to consider nonlinear response of cable-stayed structures, a closed-form refined model was proposed [26]. To simplify the dynamic analysis of emergency bridge, the equivalent modulus of elasticity (Ernst 1965) [27–30] had been used to consider the sag effect of main cable. The finite element model of the emergency bridge was established using ANSYS software. In the finite element model, the main girders and cross beam were modeled by element BEAM4. The mass and rotation inertia of middle plate focus on the middle of cross beam, which had been modeled by the element MASS21. The pylon has several cross-sections, which had been modeled by element BEAM188. Main cable and suspender were modeled by element LINK10. Boundary conditions of finite element model of the emergency bridge are shown in Table 1. Three-dimensional finite element model of the emergency bridge is shown in Figure 5. The hinge

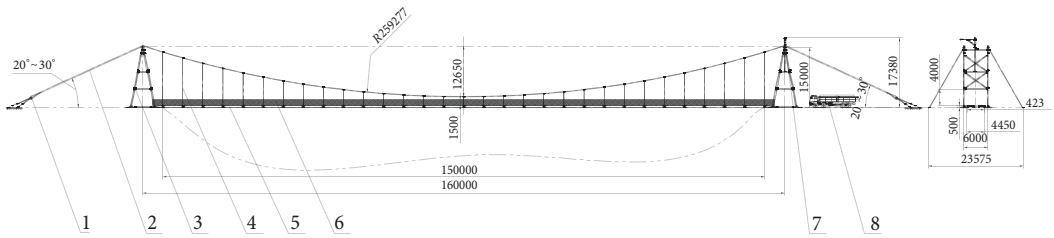

1-anchoring system; 2-main cable; 3-pylon; 4-suspender; 5-deck,
6-safety net; 7-equipment of erection of straddle; 8-carrier vehicle

(a) Lateral view

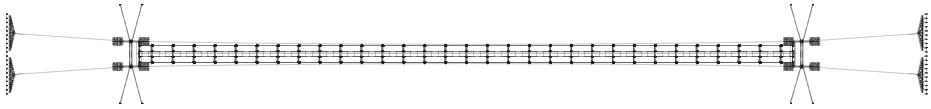

(b) Vertical view

Figure 1: General arrangement of emergency bridge.

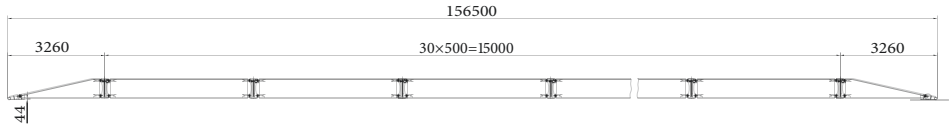

(a) Lateral view

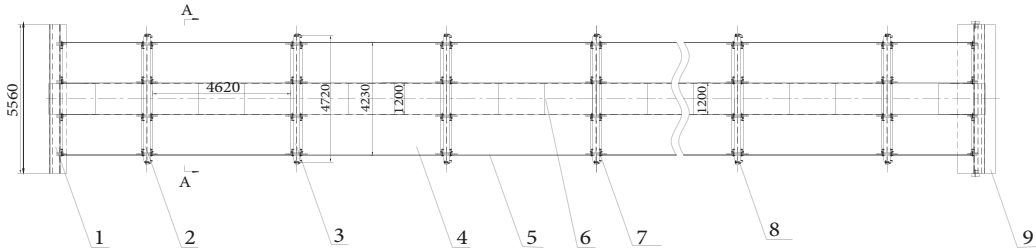

1-fixed support; 2-border girder; 3-main cross girder; 4-standard beam; 5-curb; 6-middle plate;
7-bolt of beam; 8-bolt of suspender; 9-sliding support

(b) Vertical view

Figure 2: General arrangement of emergency bridge deck.

connection between the main girders has been modeled by the method of constraint coupling. Using the Lanczos method in ANSYS, a dynamic finite-element analysis has been performed. Dynamic characteristics of the emergency bridge are shown in Table 2. The bridge flutter stability is mainly related to the first-order model of the vertical bending and torsion. The first-order vertical bending frequency is 0.509Hz, and the first-order torsion frequency is 0.846Hz. The first antisymmetric vertical bending mode and the first antisymmetric torsion mode of stiffening girder of the emergency bridge are shown in Figures 6 and 7, respectively.

3. Wind Tunnel Tests

3.1. Design of the Sectional Model. Wind tunnel tests of the section models have been carried out in the TJ-2 wind tunnel laboratory at Tongji University in China. The model scale is 1:10. So, the parameter of the section model can be obtained based on the comparability demand. The major parameters of the section model are shown in Table 3. The stringer and horizontal girder system has been used on the framework of the section model. The girder has been welded with steel. The bridge deck of the section model has been sculptured with timber. The wind fairing and baseplate are made of ABS materials. The wind tunnel test of the section model only considers two degrees of freedom of the vertical direction and the torsional direction. The section model of the emergency bridge is shown in Figure 8.

3.2. Flutter Performance of Original Emergency Bridge Scheme. Subjected to the smooth flow, the flutter critical wind speed of the original emergency bridge scheme has been measured at

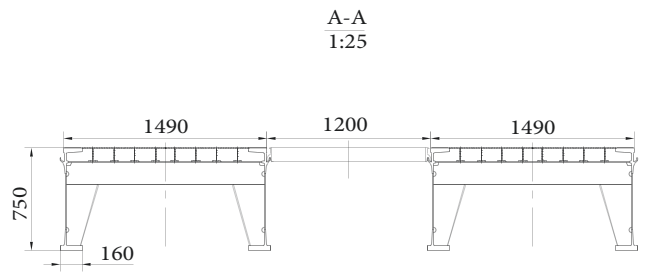

Figure 3: Cross-section of main girder (mm).

Table 1: Boundary conditions of finite element model of the emergency bridge.

Degree of freedom	UX	UY	UZ	ROTZ	ROTX	ROTY
Beam end	⊕	×	×	⊕	⊕	⊕
Bottom of pylon	×	×	×	×	×	×
Between main cable and top of pylon	CP	CP	CP	CP	CP	CP
Main cable at the anchor end	×	×	×	×	×	×

Notations represent the following. UX: the longitudinal direction, UY: the vertical direction, UZ: the lateral direction, ROTX: torsion in longitudinal direction, ROTY: torsion in vertical direction, ROTZ: torsion in lateral direction, ⊕: release the degree of freedom, ×: constraint to degree of freedom, and CP: coupling the degree of freedom.

Table 2: Dynamic characteristics results.

Mode No.	Frequency (Hz)	Mode shape description
1	0.509	1st-A-VB (MG)
2	0.635	1st-S-VB (MG)
3	0.846	1st-A-T (MG)
4	1.028	2nd-S-VB (MG)
5	1.056	1st-S-T (MG)
6	1.469	2nd-S-T (MG)
7	1.476	B (MC)
8	1.670	2nd-A-VB (MG)
9	2.075	2nd-A-T (MG)
10	2.146	B (MC)

Notations represent the following. H: horizontal, V: vertical, L: Longitudinal, B: bending, T: torsion, F: floating, S: symmetric, A: anti-symmetric, MG: main girder, MC: main cables, and P: pylon.

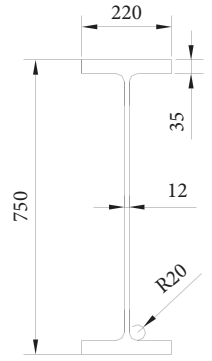

Figure 4: Cross-section of main cross girder (mm).

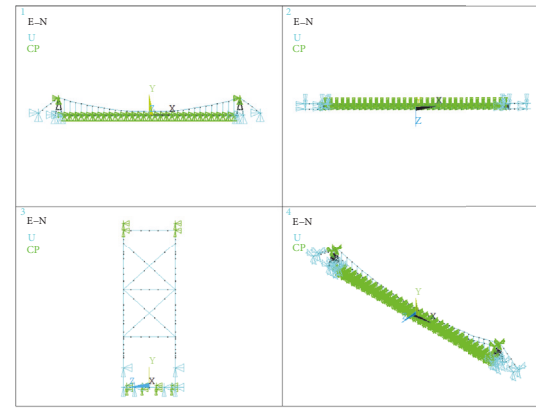

Figure 5: Finite element model of the emergency bridge.

the wind attack angles of −3°, 0°, and +3°. The data acquisition system can instantly display the data of displacement for the section model. The flutter critical wind speed is the wind speed when the state of the section model system changes from stable to unstable. The wind speed scale is the ratio between wind speed in wind tunnel test and wind speed for actual bridge; it equals the model scale divided by the ratio of torsion frequency. The wind speed scale has been used to calculate the flutter critical wind speed of the actual emergency bridge. The flutter critical wind speed of the original emergency bridge scheme at the wind attack angles of −3°, 0°, and +3° is shown in Table 4.

Based on the design requirements of the emergency bridge, the flutter checking wind speed is 20.1 m/s. The variation of the torsional damping ratio of the original scheme's section model system with wind speed is shown in Figure 9. The results show that the flutter critical wind speeds of original cross-section are less than the corresponding flutter checking wind speed at the wind attack angles of −3°, 0°, and +3°, leading to the possibilities of flutter. The stability of the original scheme against flutter is insufficient.

Table 3: Parameters of the section model.

Parameters	Units	Bridge value	Scale ratios	Section model value
Height of girder	m	0.75	1:10	0.075
Width of girder	m	4.23	1:10	0.423
Mass per unit length	kg/m	680	$1:10^2$	6.7042
Mass moment of inertia per unit length	$kg \cdot m^2/m$	1800	$1:10^4$	0.252
Radius of gyration	m	1.63	1:10	0.18
Fundamental frequency of vertical bending	Hz	0.509	2.776	1.413
Fundamental frequency of torsion	Hz	0.846	2.777	2.349
Frequency ratio of torsion and bending	/	1.662	/	1.655
Wind speed scale	m/s	/	1:3.6	/
Damping ratio of bending	%	0.5	/	0.2
Damping ratio of torsion	%	0.5	/	0.3

Table 4: Flutter critical wind speeds of original emergency bridge scheme.

Wind attack angle (°)	Flutter critical wind speed (m/s)		Corresponding flutter checking wind speed (m/s)
	Section model of the emergency bridge	Emergency bridge	
-3	2.85	10.26	20.1
0	2.625	9.45	
3	2.50	9.0	

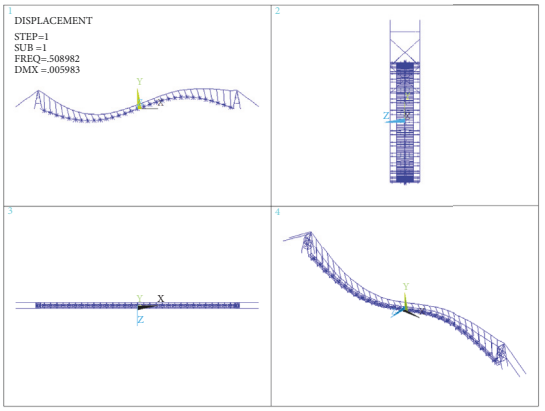

Figure 6: The first antisymmetric vertical bending mode of the stiffening girder.

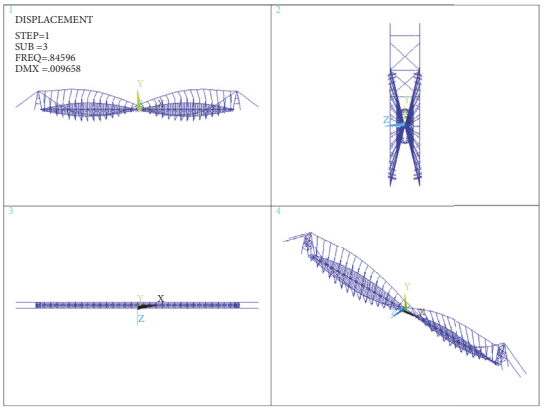

Figure 7: The first antisymmetric torsion mode of the stiffening girder.

Therefore, the flutter critical wind speed of the emergency bridge needs to be improved by structural measures or aerodynamic optimization schemes.

3.3. Flutter Optimization of the Emergency Bridge. In order to improve the flutter performance of the emergency bridge, different aerodynamic optimization schemes have been developed, which are shown in Figure 10. Section model of the emergency bridge in wind tunnel tests mainly considers vibration of two degrees of freedom (vertical vibration and torsional vibration), so the test results only give the flutter derivatives correlation with the vertical vibration and torsional vibration. Flutter derivatives of different aerodynamic schemes are shown in Figure 11. The influence of different

Figure 8: Section model of the original emergency bridge scheme.

Table 5: Descriptions of four aerodynamic optimization schemes.

Aerodynamic optimization scheme		Description of the aerodynamic optimization scheme
1	Central-slotted	Dismantle the board between the girder sides
2	Wind fairing	Install the wind fairing on both girder sides
3	Central-slotted + wind fairing	Combined Scheme 1 and Scheme 2
4	Plus bottom board + wind fairing	Plus the board under the girder and install the wind fairing

Table 6: Test results of bridge flutter critical wind speed.

Aerodynamic optimization scheme	Wind attack angle (°)	Flutter critical wind speed (m/s)	
		Section model of the emergency bridge	Emergency bridge
1	-3°	2.25	8.1
	0°	1.75	6.3
	+3°	1.62	5.8
2	-3°	5.50	19.8
	0°	5.35	19.3
	+3°	5.28	19.0
3	-3°	9.40	34.2
	0°	7.95	28.8
	+3°	6.45	24.3
4	-3°	5.85	21.1
	0°	5.69	20.5
	+3°	5.65	20.3

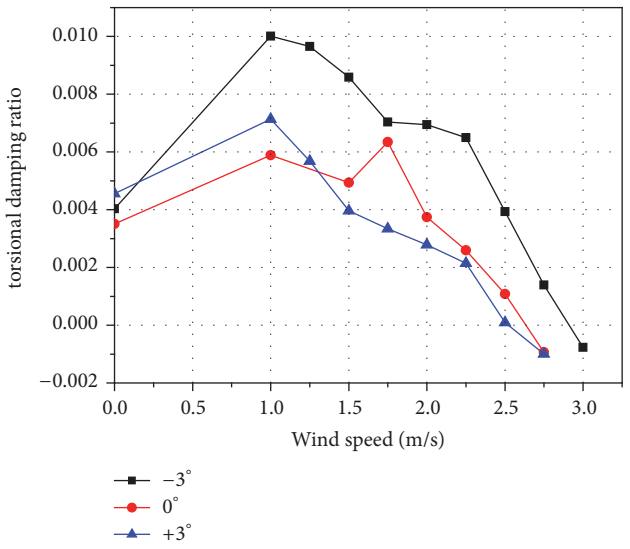

Figure 9: Variation of torsional damping ratio of the original scheme's section model system with wind speed.

aerodynamic measures to the flutter performance has been investigated. Four aerodynamic optimization schemes are shown in Table 5. The bridge flutter critical wind speeds of four aerodynamic optimization schemes at the wind attack angles of −3°, 0°, and +3° have been measured by wind tunnel tests. Due to the limited space in this paper, only damping ratio and frequency of Scheme 3 are shown in Figure 12.

In order to analyze the flutter characteristics of the emergency bridge conveniently based on the flutter mechanism, the major flutter derivatives of different schemes at the wind attack angle of 0° are shown in Figure 11. The flutter derivative A_2^* is related to the aerodynamic damping, which is generated by the torsional motion. If A_2^* is positive, it is an indication of aerodynamic negative damping, and vice versa. Figure 11 (1) shows the flutter derivative A_2^* of the original scheme and Scheme 1 changes from negative to positive with the wind speed increases. This is an indication that the aerodynamic negative damping is produced, which means the emergency bridge is less stable against flutter. The flutter derivative A_2^* of the other aerodynamic optimization schemes is negative with the wind speed increases. So, Scheme 3 is more stable than the other schemes against flutter. The flutter derivative H_2^* is related to the stiffness and damping of the vertical bending affected by the torsional velocity. The correlation between increasing H_2^* and the flutter stability is positive. Figure 11 (2) shows that H_2^* of different schemes increase with the wind speed increases. Further, H_2^* of Scheme 3 is larger than those of the other schemes. The flutter derivative A_3^* is related to the torsional stiffness, which is affected by the torsional motion. Generally, the effect of A_3^* on the flutter critical wind speed is small. Figure 11 (3) shows that different schemes have similar variation tendencies with the wind speed increase. Therefore, based on the analysis of the major flutter derivatives, the flutter stability of Scheme 3 is the best among four aerodynamic optimization schemes.

The variations of the torsional damping ratio of different schemes' section model systems with wind speed are shown in Figure 12. Based on the wind-resistance design code for highway bridges (JTG/TD60-01-2004) [31], the safety factor of the emergency bridge is 1.2. Table 6 shows the bridge flutter

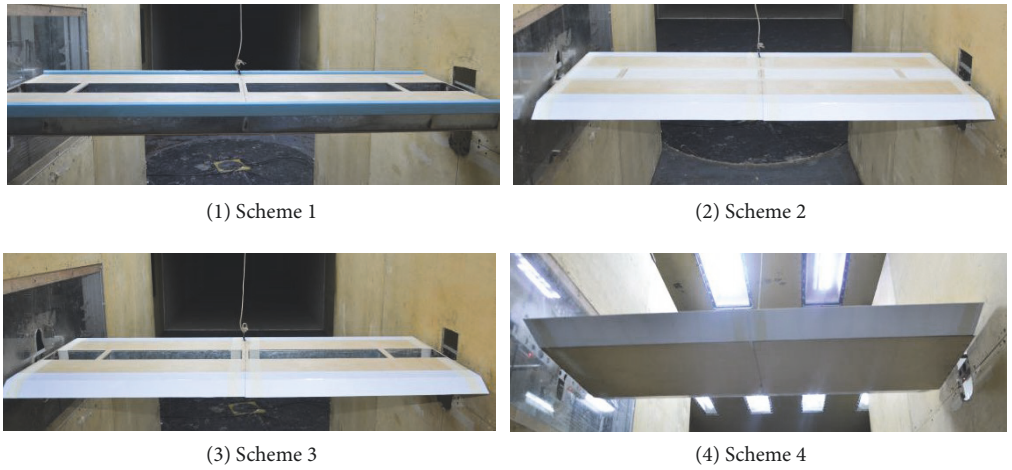

(1) Scheme 1 (2) Scheme 2

(3) Scheme 3 (4) Scheme 4

Figure 10: Section models of four aerodynamic optimization schemes.

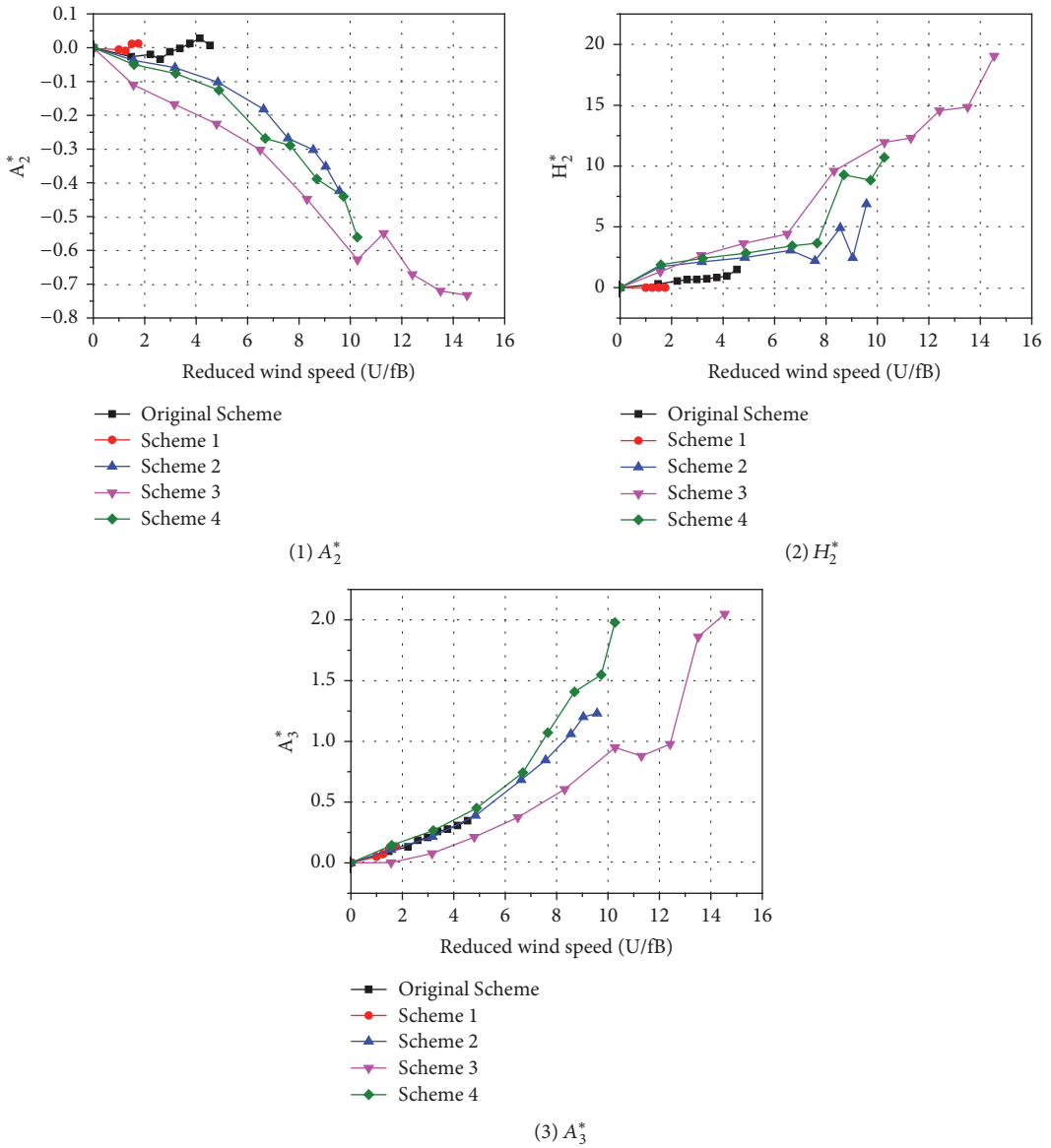

(1) A_2^* (2) H_2^*

(3) A_3^*

Figure 11: Bridge flutter derivatives of different schemes.

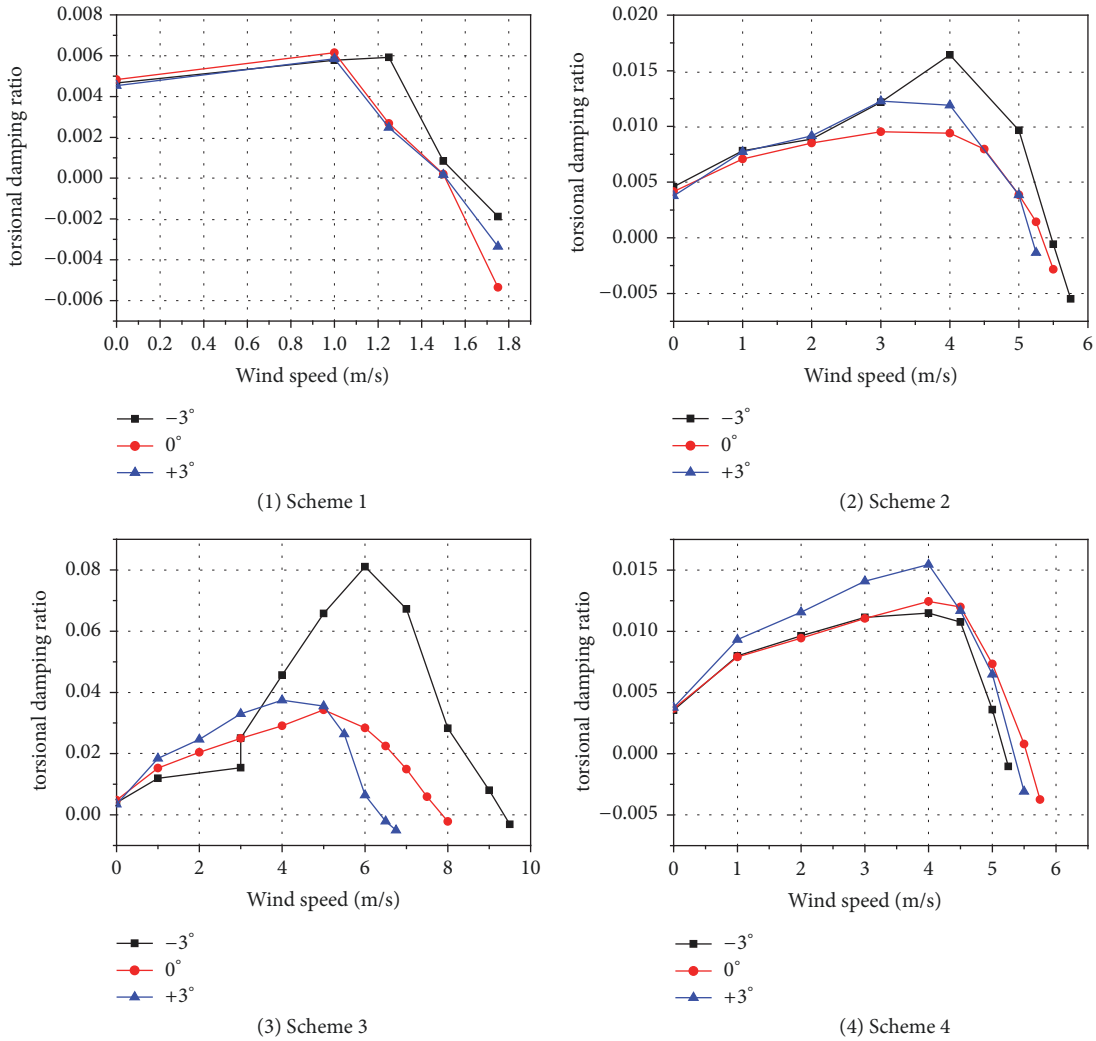

FIGURE 12: Variation of torsional damping ratio of four schemes' section model systems with wind speed.

critical wind speed of different aerodynamic optimization schemes at wind attack angles of −3°, 0°, and +3°. It can be seen that the flutter critical wind speed at wind attack angle of +3° is smaller than those at wind attack angles of −3° and 0°. So, the bridge flutter critical wind speed at the attack angle of +3° has been used for further comparison. The bridge flutter critical wind speed of the central-slotted scheme is 5.8 m/s. So, this aerodynamic measure cannot improve the flutter critical wind speed. The bridge flutter critical wind speed of the wind fairing scheme is 19.0 m/s. This is a significant improvement to the bridge flutter critical wind speed, but it still cannot meet the design requirement. The bridge flutter critical wind speed of the aerodynamic combined measurements of the central-slotted and wind fairing is 24.3 m/s; this scheme can make the flutter performance of the emergency bridge meet the requirements. The bridge flutter critical wind speed of the scheme of plus the board under the girder and install the wind fairing is 20.3 m/s. This scheme can meet the design requirement, but the safety coefficient is less than 1.2.

Summarizing the above analysis, the aerodynamic combined measurements of the central-slotted and wind fairing can make flutter performance of the emergency bridge meet the requirements. So, the aerodynamic combined measurements of the central-slotted and wind fairing are the optimal scheme in four aerodynamic optimization schemes.

4. Flutter Analysis of the Emergency Bridge

4.1. Fundamental Theory of Flutter. Based on the structural vibration theory, the equation for motion of bridge structure in steady airflow can be expressed as

$$M\ddot{X} + C\dot{X} + KX = F_a \tag{1}$$

where M is the bridge mass matrix, C is the damping matrix of the bridge, K is the stiffness matrix of bridge, X is the vector of displacement of the bridge, $\dot{X}$ is the vector of velocity of the bridge, $\ddot{X}$ is the vector of acceleration of the bridge, and F_a is the vector of aeroelastic forces on the bridge.

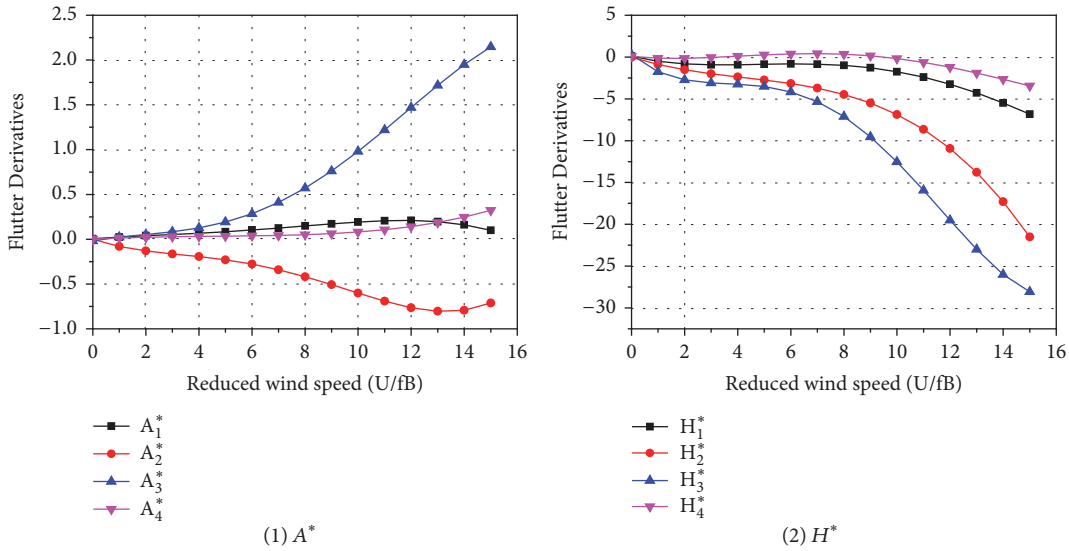

Figure 13: Flutter derivatives of the optimal aerodynamic scheme at attack angle of 0°.

Based on the flutter theory of R.H. Scanlan (1965), for a bridge structure in steady airflow, the self-excited lift force L_{se}, drag force D_{se}, and pitching moment M_{se} per unit length are defined in the following equations. Eqs. (2a)-(2c) fully consider the lateral movement of the bridge structure.

$$L_{se} = \frac{1}{2}\rho U^2 (2B)\left(KH_1^*\frac{\dot{h}}{U} + KH_2^*\frac{B\dot{\alpha}}{U} + K^2H_3^*\alpha + K^2H_4^*\frac{h}{B} + KH_5^*\frac{\dot{p}}{U} + K^2H_6^*\frac{p}{B}\right) \tag{2a}$$

$$D_{se} = \frac{1}{2}\rho U^2 (2B)\left(KP_1^*\frac{\dot{p}}{U} + KP_2^*\frac{B\dot{\alpha}}{U} + K^2P_3^*\alpha + K^2P_4^*\frac{p}{B} + KP_5^*\frac{\dot{h}}{U} + K^2P_6^*\frac{h}{B}\right) \tag{2b}$$

$$M_{se} = \frac{1}{2}\rho U^2 \left(2B^2\right)\left(KA_1^*\frac{\dot{h}}{U} + KA_2^*\frac{B\dot{\alpha}}{U} + K^2A_3^*\alpha + K^2A_4^*\frac{h}{B} + KA_5^*\frac{\dot{p}}{U} + K^2A_6^*\frac{p}{B}\right) \tag{2c}$$

where ρ, U, and B are the air density, the mean wind speed, and the width of the bridge deck, respectively; K represents the reduced circular frequency that can be expressed as $K = (\omega \cdot B)/U$. h is the vertical displacement of bridge, p is the lateral displacement of bridge, α is the torsional displacement of bridge, and the dot superscript denotes the derivative with respect to time. H_i, P_i, and A_i $(i = 1, 2, 3, 4, 5, 6)$ are the flutter derivatives related to the vertical, lateral, and torsional directions, respectively. Flutter derivatives are related to the shape of the main girder only, and they can be obtained by carrying out wind tunnel test or CFD.

Based on the thought of finite element analysis, the distributed aerodynamic forces can be converted into the equivalent nodal loadings acting on the bridge element, and the aeroelastic forces for element e can be expressed as

$$F_{ae}^e = K_{ae}^e X^e + C_{ae}^e \dot{X}^e \tag{3}$$

where X^e is the vector of nodal displacement and $\dot{X}^e$ is the vector of nodal velocity; K_{ae}^e is the local aeroelastic stiffness matrix; C_{ae}^e is the vector of the local aeroelastic damping matrix.

Matrix27 element of ANSYS software can model the stiffness component or the damping of bridge structure. So the total aeroelastic stiffness matrix of bridge K_{ae}^e and the damping matrix of bridge C_{ae}^e can be expressed as

$$K_{ae}^e = \begin{bmatrix} K_{ae1}^e & 0 \\ 0 & K_{ae1}^e \end{bmatrix}$$
$$C_{ae}^e = \begin{bmatrix} C_{ae1}^e & 0 \\ 0 & C_{ae1}^e \end{bmatrix} \tag{4}$$

$$K_{ae1}^e = a\begin{bmatrix} 0 & 0 & 0 & 0 & 0 & 0 \\ 0 & P_6^* & P_4^* & BP_3^* & 0 & 0 \\ 0 & H_6^* & H_4^* & BH_3^* & 0 & 0 \\ 0 & BA_6^* & BA_4^* & B^2A_3^* & 0 & 0 \\ 0 & 0 & 0 & 0 & 0 & 0 \\ 0 & 0 & 0 & 0 & 0 & 0 \end{bmatrix} \tag{5}$$

$$C_{ae1}^e = b\begin{bmatrix} 0 & 0 & 0 & 0 & 0 & 0 \\ 0 & P_5^* & P_1^* & BP_2^* & 0 & 0 \\ 0 & H_5^* & H_1^* & BH_2^* & 0 & 0 \\ 0 & BA_5^* & BA_1^* & B^2A_2^* & 0 & 0 \\ 0 & 0 & 0 & 0 & 0 & 0 \\ 0 & 0 & 0 & 0 & 0 & 0 \end{bmatrix} \tag{6}$$

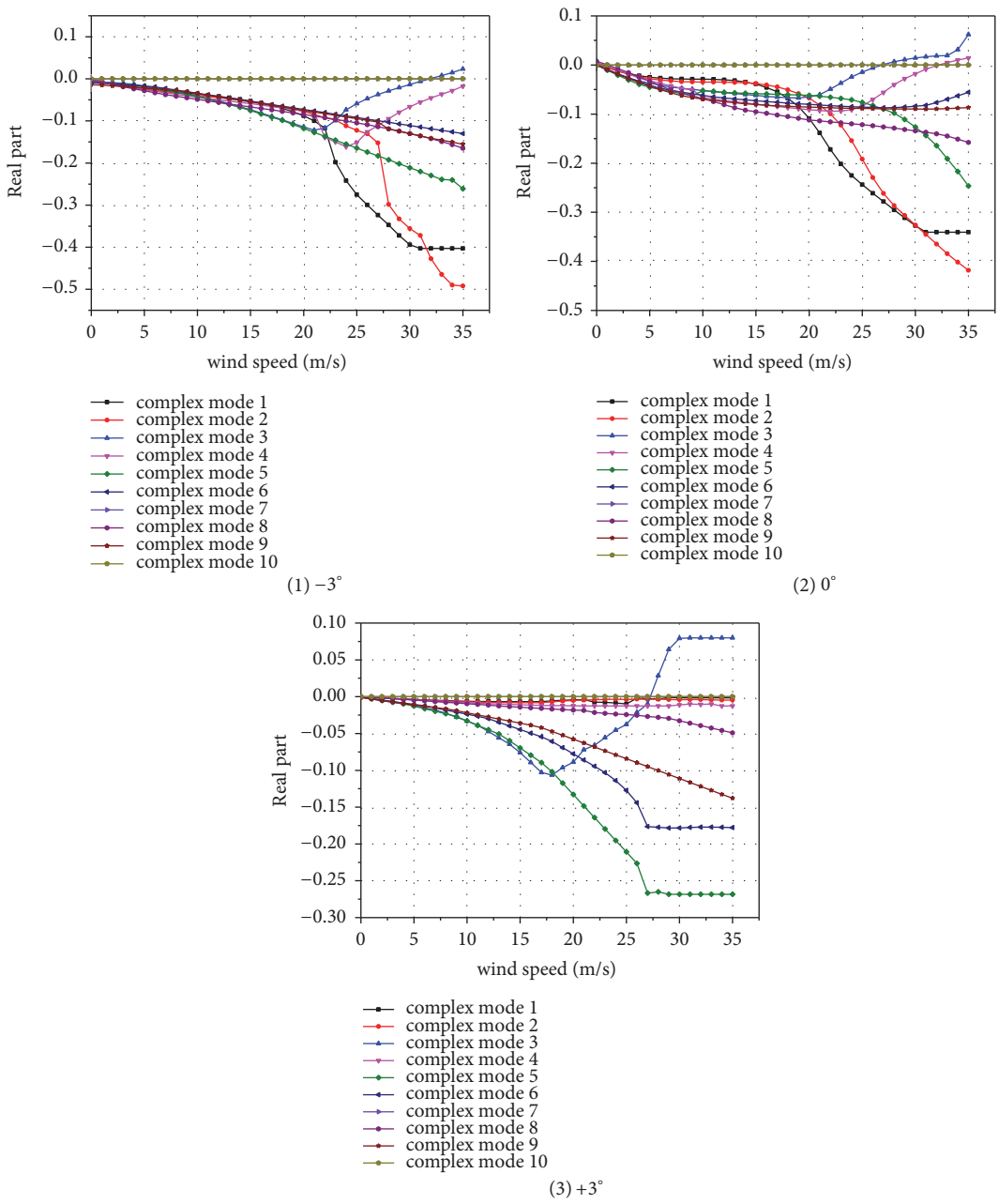

Figure 14: Variation of damping ratio of the emergency bridge with wind speed at attack angles of −3°, 0°, and +3°.

where $a = \rho U^2 K^2 Le/2$; $b = \rho UBKLe/2$, and Le is the length of element e.

The global aeroelastic stiffness and damping matrices can be obtained by equation (7).

$$F_{ae} = K_{ae}X + C_{ae}\dot{X} \tag{7}$$

where K_{ae} represents the global aeroelastic stiffness matrix, and C_{ae} represents the global aeroelastic damping matrix.

Substituting Eq. (7) into Eq. (1) leads to the equation of motion for the bridge structure, as follows:

$$M\ddot{X} + \left(C - C_{ae}\right)\dot{X} + \left(K - K_{ae}\right)X = 0 \tag{8}$$

The equation of motion of bridge structure for flutter analysis can be obtained after incorporating the Rayleigh structure damping matrix assumption $C = \alpha M + \beta K$, and the equation is expressed as

$$M\ddot{X} + \left(C - C'_{ae}\right)\dot{X} + \left(K - K_{ae}\right)X = 0 \tag{9}$$

where C', C'_{ae} are the modified damping and the modified aeroelastic damping matrices, respectively. They can be expressed as

$$C' = \alpha M + \beta\left(K - K_{ae}\right) \tag{10}$$

$$C'_{ae} = C_{ae} - \beta K_{ae} \tag{11}$$

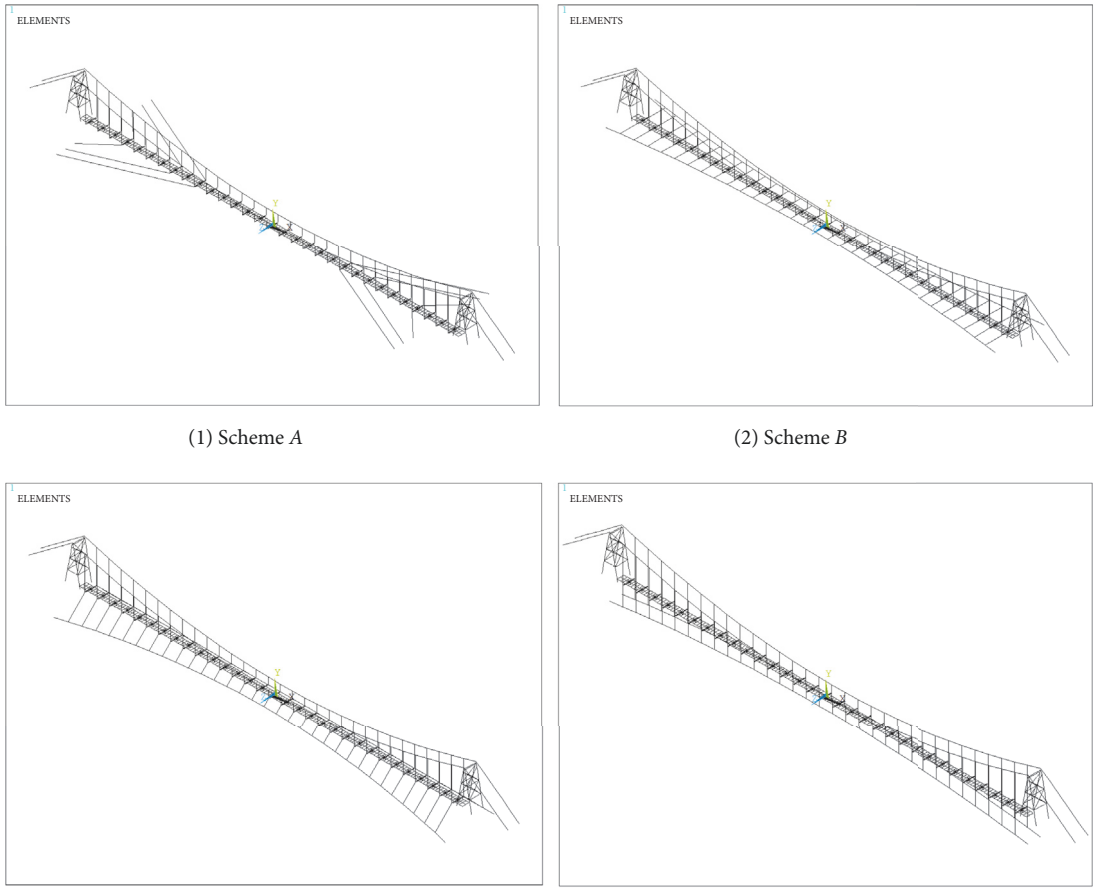

(1) Scheme *A* (2) Scheme *B*

(3) Scheme *C* (4) Scheme *D*

Figure 15: Finite element model of different wind-resistance cable schemes.

where α and β are the proportionality coefficients for Rayleigh damping. α and β can be obtained by least squares fitting, as follows:

$$\min_{\alpha,\beta} \sum_{i=1}^{m} \left(2\xi_j\omega_j - \alpha - \beta\omega_j^2\right)^2 \tag{12}$$

where ξ_i and m are the damping ratio of the ith mode and the total number of mode considered, respectively.

Eq. (9) represents an integrated system in consideration of the effect of aeroelasticity, parameterized according to wind speed and response frequency. Eq. (9) can be carried out by the damped complex eigenvalue analysis method.

If the bridge system has n degrees of freedom, n conjugate pairs of complex eigenvalues and eigenvectors will be obtained by solving Eq. (9). The jth conjugate pair of complex eigenvalues can be expressed as

$$\lambda_j = \sigma_j \pm i\omega_j \tag{13}$$

where $i = \sqrt{-1}$; σ_j represents the real part of the jth conjugate pair of complex eigenvalues, and ω_j represents the imaginary part of the jth conjugate pair of complex eigenvalues. σ_j and ω_j are the damping and the vibrating frequency of the bridge system, respectively.

When the real part of all eigenvalues is negative, the bridge system is dynamically stable; otherwise the bridge system is unstable. When the real part becomes zero, the corresponding wind speed is the critical wind speed, and it means the bridge system is on the critical state.

As shown in Eq. (5) and Eq. (6), the aeroelastic stiffness matrix and the aeroelastic damping matrix are expressed according to wind speed, response frequency, and reduced frequency; only two of them are independent. Therefore, a sweep and iterative procedure should be employed in the identification of the flutter instability state. In this study, the flutter program of the emergency bridge can be implemented in ANSYS based on the scripting language APDL.

4.2. Flutter Critical Wind Speed of the Emergency Bridge Based on Numerical Calculation. Assuming that the emergency bridge structure damping ratio is 0.5%, the flutter derivative is obtained from the wind tunnel test, and the flutter program was compiled based on the APDL language in ANSYS. The bridge flutter critical wind speeds of the optimal aerodynamic scheme at the attack angles of −3°, 0°, and +3° have been calculated. The polynomial fitting method has been used to deal with the flutter derivative data of the optimal scheme, which is convenient for the flutter derivative invoked by the

Table 7: Bridge flutter critical wind speeds.

Wind attack angle (°)	Flutter critical wind speed (m/s)		error (%)
	Results of numerical calculations	Results of wind tunnel tests	
-3	31.3	34.2	8.48
0	27.2	28.8	5.56
3	26.85	24.3	9.50

Table 8: Dynamic characteristics, flutter critical wind speed, and flutter critical frequency of four wind-resistance cable schemes at attack angle of 0°.

Scheme	Fundamental frequency of vertical bending (Hz)	Fundamental frequency of lateral bending (Hz)	Fundamental frequency of torsion (Hz)	torsion-bending moment ratio	Flutter critical wind speed (m/s)	Flutter critical frequency (Hz)
A	0.702	1.332	1.040	1.481	37.22	0.8796
B	0.542	1.355	0.848	1.565	29.17	0.6513
C	0.506	1.347	0.768	1.512	38.13	0.8563
D	0.736	1.345	1.12	1.522	41.98	0.9338

flutter analysis program. The fitting derivative curves are shown in Figure 13.

As shown in Figure 14, the damping ratio and frequency at different attack angle change with the wind speed increase. As shown in Figure 14, the damping ratio of the third order vibration is the first to decrease to zero as the wind speed increases. So, the control mode of the flutter for the emergency bridge is the first order antisymmetric torsion. For the optimal scheme, the bridge flutter critical wind speeds at the wind attack angles of −3°, 0°, and +3° have been calculated by the flutter program, and the results are shown in Table 7; the results agree well with the wind tunnel test results. The maximum error is 9.5%. So, the flutter program can be used for flutter analysis of an emergency bridge.

The flutter critical wind speed of the emergency bridge at the attack angle of +3° is slower than the flutter critical wind speed at attack angles −3° and 0°. As the flutter critical wind speed is bigger than the corresponding flutter checking wind speed, the emergency bridge is still not safe. So, other structural measures should be applied in order to further improve the flutter stability of the emergency bridge.

4.3. Effect of Wind-Resistance Cable Structure on the Flutter Critical Wind Speed of the Emergency Bridge. The flutter derivative is a dimensionless parameter which only relates to the sectional shape [32, 33]. The flutter derivative can reflect the aerodynamic characteristics of a section. Ignore the influence of a wind-resistance cable in a flow field; the flutter derivative does not change when the section shape remains unchanged. In order to improve the safety of the emergency bridge in the regions of complex topography, four different wind-resistance cable schemes have been developed, which are shown in Figure 15. Using the flutter program, the bridge flutter critical wind speeds of different wind-resistance cable schemes have been calculated, and the optimal scheme has been determined.

Scheme *A*: the wind-resistance cable is added symmetrically in the horizontal direction at the locations $L/4$, $L/8$, and $3L/16$ of the emergency bridge (L represents the span of the emergency bridge). The initial strain of the wind-resistance cable is 0.003, and the wind-resistance cable is anchored to the rock.

Schemes *B*, *C*, and *D*: the wind-resistance cable in an arch shape has been installed on both sides of the emergency bridge. The wind-resistance cable and the main girder are connected by a tension rod. At mid-span, the length of the tension rod between the wind-resistance cable and the main girder is 1 m. At other locations, the length of tension rod depends on the rise-span ratio of the emergency bridge. The initial strain of the wind-resistance cable is 0.003. The relative positions of the wind-resistance cable and the emergency bridge deck for Schemes B, C, and D are 0°, 45°, and 90°, respectively.

The dynamic characteristics and flutter critical wind speed of different wind-resistance cable schemes at the attack angle of 0° are shown in Table 8. The results indicate that the flutter critical wind speed is positively correlated with the torsional frequency. The critical wind speed of Scheme D is 41.98 m/s which is larger than those of the other three wind-resistance cable schemes. As compared to the emergency bridge without the wind-resistance cable, the bridge flutter critical wind speed increased 31.4%. In consideration of the convenience in construction and the effectiveness in erection, Scheme *A* has been selected. The flutter critical wind speed of Scheme A can meet the requirements of flutter stability. Hence, the emergency bridge possesses sufficient security against flutter.

5. Conclusions

The flutter critical wind speed of the original emergency bridge scheme is slower than the corresponding flutter checking wind speed at the wind attack angles of −3°, 0°, and +3°, leading to the possibilities of flutter. Based on the

original scheme, four aerodynamic optimization schemes have been developed. Based on the wind tunnel test results, the aerodynamic combined measurements of central-slotted and wind fairing are the optimal scheme, which can make the flutter critical wind speed and the safety coefficient of the bridge meet the design requirements of the emergency bridge at the wind attack angles of -3°, 0°, and $+3^{\circ}$. The flutter program has been compiled using the APDL language. The calculated flutter critical wind speed results by the flutter program agree well with the wind tunnel test results. The maximum error is only 9.5%. In order to improve the flutter stability of the emergency bridge, the critical wind speeds of different wind-resistance cable schemes have been calculated by the flutter analysis program. The results show that the scheme of wind-resistance cable in the horizontal direction can meet the requirement of flutter stability, which is also convenient in constructing and effective in erecting an emergency bridge.

Data Availability

The datasets generated and analyzed during this study are available from the corresponding author on reasonable request.

Conflicts of Interest

The authors declared that they have no conflicts of interest to this work.

Acknowledgments

The research described in this paper is funded by projects (No. 2016M602972 and No. 2018M643852) supported by the Postdoctoral Science Foundation of China and project (No. 30110010403) supported by the Advanced Research Program on Equipment of China. This support is gratefully acknowledged.

References

[1] R. H. Scanlan, "Problematics in formulation of wind-force models for bridge decks," *Journal of Engineering Mechanics*, vol. 119, no. 7, pp. 1353–1375, 1993, American Society of Civil Engineers.

[2] N. N. Dung, T. Miyata, H. Yamada, and N. N. Minh, "Flutter responses in long span bridges with wind induced displacement by the mode tracing method," *Journal of Wind Engineering & Industrial Aerodynamics*, vol. 77-78, pp. 367–379, 1998.

[3] Y. J. Ge and H. Tanaka, "Aerodynamic flutter analysis of cable-supported bridges by multi-mode and full-mode approaches," *Journal of Wind Engineering & Industrial Aerodynamics*, vol. 86, no. 2-3, pp. 123–153, 2000.

[4] R. H. Scanlan and N. P. Jones, "Aeroelastic analysis of cable-stayed bridges," *Journal of Structural Engineering (United States)*, vol. 116, no. 2, pp. 279–297, 1990.

[5] A. Jain, N. P. Jones, and R. H. Scanlan, "Coupled aeroelastic and aerodynamic response analysis of long-span bridges," *Journal of Wind Engineering & Industrial Aerodynamics*, vol. 60, no. 1-3, pp. 69–80, 1996.

[6] H. Tanaka, N. Yamamura, and M. Tatsumi, "Coupled mode flutter analysis using flutter derivatives," *Journal of Wind Engineering & Industrial Aerodynamics*, vol. 42, no. 1-3, pp. 1279–1290, 1992.

[7] G. Vairo, "A numerical model for wind loads simulation on long-span bridges," *Simulation Modelling Practice and Theory*, vol. 11, no. 5-6, pp. 315–351, 2003.

[8] F. Maceri and G. Vairo, "Modelling and simulation of long-span bridges under aerodynamic loads," in *Engineering Structures*, vol. 14 of *Lecture Notes in Applied and Computational Mechanics*, pp. 359–381, Springer, Berlin, Germany, 2004.

[9] S. de Miranda, L. Patruno, F. Ubertini, and G. Vairo, "On the identification of flutter derivatives of bridge decks via RANS turbulence models: Benchmarking on rectangular prisms," *Engineering Structures*, vol. 76, pp. 359–370, 2014.

[10] F. Nieto, J. S. Owen, D. M. Hargreaves, and S. Hernández, "Bridge deck flutter derivatives: Efficient numerical evaluation exploiting their interdependence," *Journal of Wind Engineering & Industrial Aerodynamics*, vol. 136, pp. 138–150, 2015.

[11] M. Ricci, L. Patruno, S. de Miranda, and F. Ubertini, "Effects of low incoming turbulence on the flow around a 5 : 1 rectangular cylinder at non-null-attack angle," *Mathematical Problems in Engineering*, vol. 2016, Article ID 2302340, 12 pages, 2016.

[12] L. Patruno, "Accuracy of numerically evaluated flutter derivatives of bridge deck sections using RANS: Effects on the flutter onset velocity," *Engineering Structures*, vol. 89, pp. 49–65, 2015.

[13] X. Zhang, H. Xiang, and B. Sun, "Nonlinear aerostatic and aerodynamic analysis of long-span suspension bridges considering wind-structure interactions," *Journal of Wind Engineering & Industrial Aerodynamics*, vol. 90, no. 9, pp. 1065–1080, 2002.

[14] X. Hua, Z. Chen, Y. Ni, and J. Ko, "Flutter analysis of long-span bridges using ANSYS," *Wind and Structures, An International Journal*, vol. 10, no. 1, pp. 61–82, 2007.

[15] W. M. Zhang, Y. J. Ge, and M. L. Levitan, "Aerodynamic flutter analysis of a new suspension bridge with double main spans," *Wind and Structures, An International Journal*, vol. 14, no. 3, pp. 187–208, 2011.

[16] G. Vairo, "A simple analytical approach to the aeroelastic stability problem of long-span cable-stayed bridges," *International Journal for Computational Methods in Engineering Science and Mechanics*, vol. 11, no. 1, pp. 1–19, 2010.

[17] H. Bai, Y. Li, and J. W. Li, "Flutter stability of a steel truss girder suspension bridge," *Shock and Vibration*, vol. 32, no. 4, pp. 90–95, 2013 (Chinese).

[18] Z. W. Zhu, S. L. He, and X. G. Hua, "Three-dimensional flutter analysis of a suspension bridge with PC slab stiffening girder," *Shock and Vibration*, vol. 31, no. 3, pp. 13–17, 2012 (Chinese).

[19] Y. Yang, R. Zhou, Y. Ge, X. Zou, and L. Zhang, "Flutter characteristics of twin-box girder bridges with vertical central stabilizers," *Engineering Structures*, vol. 133, pp. 33–48, 2017.

[20] H. J. Tang, K. M. Shum, and Y. L. Li, "Investigation of flutter performance of a twin-box bridge girder at large angles of attack," *Journal of Wind Engineering & Industrial Aerodynamics*, vol. 186, pp. 192–203, 2019.

[21] G. Caruso, G. Chirianni, and G. Vairo, "Energy harvesting from wind-induced bridge vibrations via electromagnetic transduction," *Engineering Structures*, vol. 115, pp. 118–128, 2016.

[22] Y. Ge, Y. Chang, L. Xu, and L. Zhao, "Experimental investigation on spatial attitudes, dynamic characteristics and environmental

conditions of rain–wind-induced vibration of stay cables with high-precision raining simulator," *Journal of Fluids and Structures*, vol. 76, pp. 60–83, 2018.

[23] F. Rizzo, L. Caracoglia, and S. Montelpare, "Predicting the flutter speed of a pedestrian suspension bridge through examination of laboratory experimental errors," *Engineering Structures*, vol. 172, pp. 589–613, 2018.

[24] Y. Y. Huang, "Study on anti-wind design for long-span and high-pier emergency steel bridge," *Journal of Railway Engineering Society*, vol. 14, no. 2, pp. 37–48, 1997 (Chinese).

[25] G. Vairo, "A quasi-secant continuous model for the analysis of long-span cable-stayed bridges," *Meccanica*, vol. 43, no. 2, pp. 237–250, 2008.

[26] G. Vairo, "A closed-form refined model of the cables' nonlinear response in cable-stayed structures," *Mechanics of Advanced Materials and Structures*, vol. 16, no. 6, pp. 456–466, 2009.

[27] H. J. Ernst, "Der E-modul von seilen unter Beruecksichtigung des durchhanges," *Der Bauingenieur*, vol. 40, no. 2, pp. 52–55, 1965.

[28] W. Xiong, C. S. Cai, R. Xiao, and L. Deng, "Concept and analysis of stay cables with a CFRP and steel composite section," *KSCE Journal of Civil Engineering*, vol. 16, no. 1, pp. 107–117, 2012.

[29] D. Bruno, F. Greco, P. Nevone Blasi, and E. Bianchi, "A 3D nonlinear static analysis of long-span cable stayed bridges," *Annals of Solid and Structural Mechanics*, vol. 5, no. 1-2, pp. 15–34, 2013.

[30] S. J. Sun, *Study on mechanical properties of the super-span suspension bridge with CFRP cables [Ph.D. thesis]*, University of Chang'an, 2013 (Chinese).

[31] Zhongjiao highway planning and design institute, *Wind-Resistant Design Specification for Highway Bridge*, China Communication Press, Beijing, China, 2004, JTG/T D60-01-2004.

[32] R. X. Zhang, *Theoretical and experimental research on identification of flutter derivatives of bridge deck [Ph.D. thesis]*, University of Tongji, 1998 (Chinese).

[33] R. X. M Gu, Zhang., and H. F. Xiang, "Identification of flutter derivatives of bridge deck and the effects of the model parameters," *Journal of Vibration Engineering*, vol. 10, no. 4, pp. 420–426, 1998 (Chinese).